On the Lyapunov spectrum of an ensemble of vortices

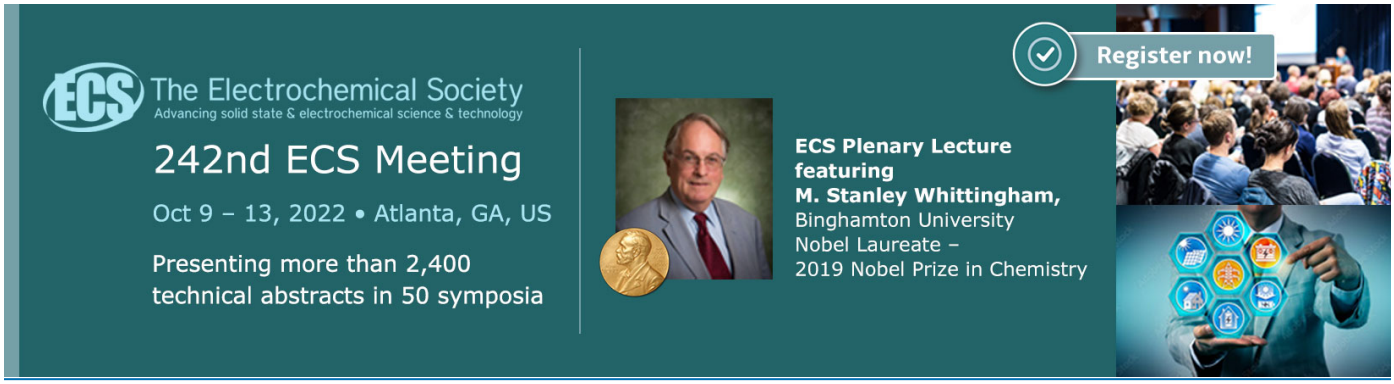

On the Lyapunov spectrum of an ensemble of vortices

L van Veen[1], **A Vela Martín**[2], **G Kawahara**[3,]

[1] Faculty of Science, Ontario Tech University, Oshawa, Ontario, Canada
[2] School of Aeronautics, Universidad Politécnica de Madrid, Madrid, Spain
[3] Graduate School of Engineering Science, Osaka University, Toyonaka, Osaka, Japan

E-mail: lennaert.vanveen@uoit.ca

Abstract. In space- and time-dependent dynamical systems, Lyapunov vectors correspond to spatio-temporal patterns of instability. These patterns can be used to parse and predict the interaction and break-down of coherent structures. The computation of Lyapunov vectors, however, is computationally demanding and has hitherto been restricted to systems with a comparatively low attractor dimension. We aim to study the dynamics of vortices in developed turbulence with an attractor dimension of order O(100). To this end, we compute the linear stability spectrum of an unstable periodic orbit embedded in the turbulent attractor and consider it a proxy for the Lyapunov spectrum. Along the periodic orbit at least 25 Lyapunov vectors can give the largest growth rate locally in time and space. We highlight one instance of a mutually induced instability of a vortex pair localized in the high-strain interstitial region.

MSC Primary: 37L30, 76D17; Secondary: 76F20.
Key words: Lyapunov spectrum, vortex flows, dynamical systems approach to turbulence.

1. Introduction

One of the most promising directions in turbulence research is the decomposition of turbulent flows into coherent structures, i.e. structures that are advected with the flow and remain coherent on a time scale much longer than that of apparently random, small-scale fluctuations (see, e.g., [1] for a discussion). One of the simplest and most common examples of a coherent structure is a vortex. Vortices can often been observed by eye in flows with tracer particles and can be identified in simulations, for instance as lines along which the pressure is minimal, or as isosurfaces of vorticity. The "decomposition" of turbulent flows into interacting vortical structures has greatly advanced our understanding of turbulent dynamics. An example of an open question addressed using vortical structures as building blocks is the search for solutions to the Navier-Stokes equation that develop singularities in finite time. Several candidate solutions have been specified in terms of vortices, such as colliding vortex rings [2] and arrays of vortex tubes [3]. In these solutions, vortical structures are created, interact and break down. We aim to explore these dynamical processes by means of its linear stability properties as measured by the Lyapunov spectrum.

M. A. Lyapunov conducted the first comprehensive study of the stability of dynamical systems to perturbations at the end of the nineteenth century [4]. He considered a general dynamical

system with n Degrees Of Freedom (DOF) and the corresponding linearization:

$$\dot{x} = f(x), \qquad \dot{v} = Df(x)v, \tag{1}$$
$$x(0) = x_0 \quad , \qquad v(0) = v_0. \tag{2}$$

The second equation is linear but depends on the solution $x(t)$, which we will refer to as the *base orbit*. Lyapunov focused on the cases in which the base orbit is an equilibrium or periodic in time. In these cases, the stability of the base orbit is determined by the eigenvalues of the Jacobian Df, and those of the *monodromy matrix*, which maps perturbations over one period, respectively. The general situation was later addressed by Oseledets' *multiplicative ergodic theorem* [5]. In a simplified form, the theorem states that there are n characteristic exponents $\Lambda_1 \geq \Lambda_2 \geq \ldots \geq \Lambda_n$ – often called Lyapunov exponents – associated with system (1-2). These exponents are found from the limits

$$\Lambda_i = \lim_{T\to\infty} \frac{1}{T} \ln \frac{\|v^{(i)}(T)\|}{\|v_0^{(i)}\|}, \tag{3}$$

where the initial perturbations $v_0^{(i)} \in V$ satisfy specific conditions. To be more specific, there exists a sequence of linear sub spaces $V^i \subsetneq V^{i-1} \subsetneq \ldots \subsetneq V^1$ such that, for every $v_0^{(i)} \in V^i \setminus V^{i+1}$ the limit converges to Λ_i. If at least one of the Lyapunov exponents is positive, the base orbit is chaotic. The perturbation vectors $v^{(i)}$ are called the *Lyapunov vectors*.

Attempts to turn Lyapunov's and Oseledets' theory of stability into a constructive, computational technique have partially succeeded. The computation of the leading Lyapunov pair $(v^{(1)}, \Lambda_1)$ is easy. One can start with a randomly chosen perturbation vector, and normalize it to unit length at regular intervals to avoid overflow errors. The average of the logarithms of the scaling factors then converges to Λ_1, and the perturbation vector approaches $v^{(1)}$. However, there is no straightforward way to compute the other Lyapunov pairs. In the mid nineteen eighties, two methods were published for the numerical computation of all Lyapunov exponents of a given dynamical system [6, 7]. They both rely on the observation that, if one integrates p linearly independent perturbation vectors, their span will approach that of the first p Lyapunov vectors. Also, the volume of a hypervolume spanned by the perturbation vectors will, on the average, grow as $\exp([\Lambda_1 + \ldots + \Lambda_p]t)$. However, all perturbation vectors will align with the leading Lyapunov vector exponentially fast and, in finite accuracy arithmetic, soon cease to form a proper basis. This problem is addressed by orthogonalization at regular intervals.

The basic algorithm is shown in Fig. 1. It has been widely used in computational dynamical systems – suffice it to say that the papers by Sano and and Wolf *et al.* [6, 7] have garnered over 6000 citations together. It has, however, two main drawbacks. Firstly, numerical error is amplified, especially if the magnitudes of the exponents differ greatly. In that case, the vector resulting from the Gram-Schmidt orthogonalization will be small in magnitude and in step (iii) the round-off error is amplified. This problem is exacerbated by the fact that the time averages converge at a slow rate – usually $1/\sqrt{t}$. Secondly, only the leading Lyapunov vector produced by the algorithm is *covariant*, e.g. it is a solution to the linearized equations for all time. The other vectors change discontinuously after every interval δ.

An algorithm for the computation of the Lyapunov vectors was introduced by Ginelli *et al.* [8, 9]. Their algorithm is based on that of Wolf *et al.* [7], but stores the projection coefficients computed in step (i) along a forward trajectory. Using this information, perturbation vectors can be propagated backward in time. During the back propagation, the vectors w_i converge to the Lyapunov vectors. The algorithm has been used successfully to investigate, for example, degrees of hyperbolicity in collective dynamics [10]. The bottleneck for implementation is the amount of memory required. Every time the orthogonalization is applied in forward time, or undone in backward time, the corresponding projection coefficients are stored. The number of

1. Randomly pick p orthonormal vectors $\{w_i\}_{i=1}^p$. Initialize p scalars $\{\ell_i\}_{i=1}^p = 0$; $t = 0$.
2. Repeat until convergence:
   a. Time-step system (1) over interval δ for x and each perturbation $v_0 = w_i$; $t \leftarrow t+\delta$.
   b. $\ell_1 \leftarrow \ell_1 + \ln \|w_1(\delta)\|$
   c. $w_1 \leftarrow w_1/\|w_1\|$
   d. For $j = 2, \ldots, p$
      Gram-Schmidt
      i. $w_j \leftarrow w_j - \sum_{k=1}^{j-1} (w_j \cdot w_k)\, w_k$
      ii. $\ell_j \leftarrow \ell_j + \ln \|w_j(\delta)\|$
      iii. $w_j \leftarrow w_j/\|w_j\|$
   e. Update $\Lambda_i \leftarrow \ell_i/t$ $(i = 1, \ldots, p)$

Figure 1. Wolf's algorithm [7] for the computation of Lyapunov exponents.

times this needs to be done is determined by the rate of convergence towards the Lyapunov vectors which, in turn, is set by the spectral gap between consecutive Lyapunov exponents. In discretized, dissipative Partial Differential Equations (PDEs) these gaps often shrink to zero as the resolution of the discretization is increased.

In conclusion, none of the available algorithms can be expected to yield more than the leading Lyapunov vector connected to turbulent vortical dynamics, described by a dynamical system with millions of DOF. At the same time, there are strong indications that important physical information can be obtained from the rest of the spectrum. In fact, theoretical musings on the Lyapunov spectrum of turbulence date back to the nineteen eighties when Ruelle published his landmark paper on the distribution of exponents and its dependence on the Reynolds number [11]. He focused mainly on the question of whether the density of exponents at zero, indicating neutral stability, will stay finite in the limit of infinite Reynolds number. To make predictions, he needed to make an assumption on the distribution of coherent structures over length scales through a so-called β-model. The outcome depends, however, on a model parameter that is not known with sufficient accuracy. Attempts to verify his predictions through numerical computations soon followed [12, 13]. These attempts were frustrated by the computational demands as they required both a high spatial resolution and a long run time. A conclusion the two works have in common, is that the number of unstable exponents is in the order of hundreds even for marginally turbulent flows. Based on studies of a shell model of turbulence, Yamada and Ohkitani [14] hypothesized that coherent structures in the inertial range are associate both with a group of positive Lyapunov exponents and with a group of negative ones, thus possessing a hyperbolic structure. More recently, Inubushi *et al.* [15] used the algorithm by Ginelli *et al.* [9] to study transitional shear flow and they found that all of the unstable Lyapunov pairs can make significant contributions to the dynamics.

In the current work, we make two modelling assumptions to avoid the main obstacles in the computation of the Lyapunov spectrum of turbulence:

(i) Rather than Navier-Stokes flow, we consider Large Eddy Simulation (LES), which provides a good approximation of turbulence without explicitly resolving motion on the smallest scales. The number of DOF in LES can be an order of magnitude smaller than that in Direct Numerical Simulation (DNS) of Navier-Stokes flow with similar statistical properties.

(ii) Rather than an open, chaotic base orbit, we consider an Unstable Periodic Orbit (UPO). The linear stability spectrum we consider is thus the Floquet spectrum and can be obtained as

the eigenspectrum of the monodromy matrix, i.e. the matrix that maps initial perturbations over one period.

These, admittedly strong, assumptions allow us a first look at the growth of perturbations in time and space and their relation to vortical dynamics.

2. Periodic flow with the properties of turbulence

We study an incompressible LES fluid on a triply periodic domain subject to constant external forcing. The resulting equations are

$$\partial_t u + u\cdot\nabla u + \nabla\left(\frac{p}{\rho} + \frac{1}{3}\Pi\right) - 2\nabla\cdot(\nu_T S) = \gamma f, \tag{4}$$

$$\nabla\cdot u = 0, \tag{5}$$

where u, p and S are the grid-scale velocity, pressure and rate-of-strain tensor, respectively, and Π contains the normal sub grid stress. The density, ρ, the forcing, f, and its amplitude, γ, are constant. Using the closure proposed by Smagorinsky [16], the eddy viscosity is given by

$$\nu_T = (C_\mathrm{S}\Delta)^2\sqrt{2S_{ij}S_{ij}}\,, \tag{6}$$

where C_S is the Smagorinsky parameter, Δ is the grid spacing and summation over repeated indices is implied. In the following, we will fix $\gamma = 4$ and $C_\mathrm{S} = 0.55$. While energy is removed from the system in an artificial way, this closure has been shown to faithfully reproduce inertial range dynamics and statistics, including spatial intermittency, in the presence of periodic boundary conditions (see, e.g., [17]).

The force is $f = (-\sin(x)\cos(y), \cos(x)\sin(y), 0)^T$ on a $2\pi \times 2\pi \times 2\pi$ periodic cube. The governing equations inherit the symmetries of this force so they are equivariant under translations in the z-direction. Results below are scaled with the integral length scale, the root-mean-squared velocity and the large-eddy turnover time, defined respectively by

$$L = \left\langle \frac{3\pi}{4K}\int_0^\infty k^{-1}E(k,t)\,\mathrm{d}k \right\rangle_\mathrm{t}, \qquad U^2 = \frac{2}{3}\langle K\rangle_\mathrm{t}, \qquad T = \frac{L}{U}. \tag{7}$$

Here, $K = \langle u^2\rangle_\mathrm{s}/2$, $E(k,t)$ is energy spectrum and $\langle . \rangle_{\mathrm{s,t}}$ stands for the average in space (s), time (t), or both (st). These scales are commonly used in the study of homogeneous, isotropic turbulence and we adopt them here for compatibility, even though the forcing is anisotropic. The local rate of energy transfer to the sub-grid scales is denoted by $\epsilon = 2\nu_T S_{ij}S_{ij}$. Simulations are done with a pseudo-spectral code on 64^3 grid points, yielding a dynamical system with 230243 DOF.

In this highly nonlinear dynamical system we identified a UPO that shared many of the properties of turbulence. Quantities like the distribution of the energy dissipation rate over length scales are compared in detail in reference [18]. Here, we only show a comparison of the energy spectra measured along the UPO, in the ambient LES turbulence and in a DNS of Navier-Stokes flow on the same domain and with the same forcing. It is shown in Fig. 2 and points at a strong similarity between the periodic and turbulent flows.

3. Local expansion rates

The Lyapunov spectrum can be computed at three different levels. At the top, there are the Lyapunov exponents as defined in Eq. (3). We can consider system (1) to represent the discretized LES equations, with v a finite-dimensional perturbation vector and $\|.\|$ the Euclidean

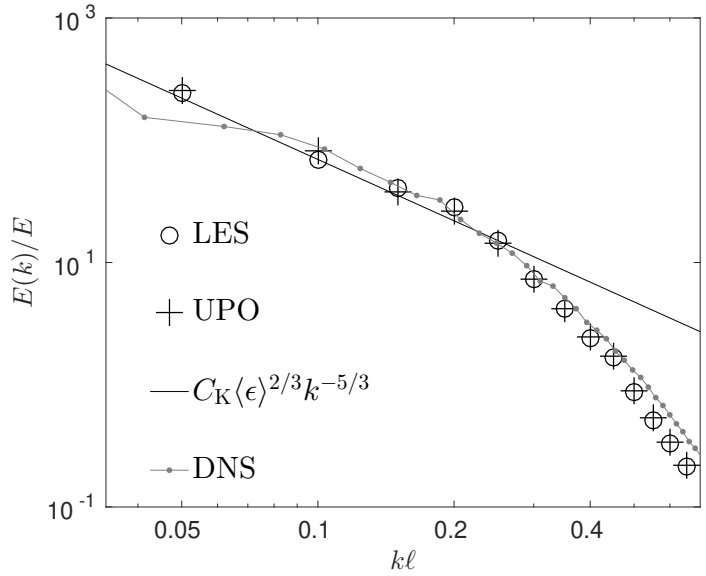

Figure 2. The time-mean energy spectrum of the UPO. For comparison the time-mean spectrum of turbulent LES and DNS, the latter with $Re_\lambda = 111$, have been included, as well as the theoretically expected Kolmogorov spectrum with $C_K = 1.5$. The small-scale nondimensionalization is given by $E = [\langle\epsilon\rangle_{st}\langle\nu_T\rangle_{st}^5]^{1/4}$ and $\ell = [\langle\nu_T\rangle_{st}^3/\langle\epsilon\rangle_{st}]^{1/4}$ for LES and $E = [\langle D\rangle_{st}\nu^5]^{1/4}$ and $\ell = [\nu^3/\langle D\rangle_{st}]^{1/4}$ for DNS, where D is the energy dissipation rate.

vector norm. Alternatively, we can consider $v = v(x,t)$ to be a perturbation field that satisfies the linearized LES equations

$$\partial_t v + u\cdot\nabla v + v\cdot\nabla u + \nabla\left(\frac{q}{\rho} + \frac{1}{3}\frac{\delta\Pi}{\delta u}v\right) - 2\nabla\cdot\left(2\frac{C_S^4\Delta^4}{\nu_T}\mathrm{Tr}(SZ)S + \nu_T Z\right) = 0, \tag{8}$$

$$\nabla\cdot v = 0, \tag{9}$$

and use the L_2 norm. In this equation, q is the perturbation pressure, Z is the perturbation rate-of-strain and $\delta\Pi/\delta u$ is the Fréchet derivative of the sub-grid stress. The exponents Λ_i then measure the time-mean growth rate of perturbations.

More detailed information can be gleaned from the *time-local* exponents defined by

$$\lambda_i = \frac{\mathrm{d}}{\mathrm{d}t}\ln\|v_i(t)\|. \tag{10}$$

Computations by van Veen *et al.* [19] and Inubushi *et al.* [15] indicate that, even in marginally turbulent flow, the time-local exponent that gives rise to the largest Lyapunov exponent on average is not the largest at every point along the base orbit. At different time instants, different instabilities dominate. Even more information about the instabilities is carried by the *Lyapunov*

fields described by the equation

$$\frac{1}{2}D_t\|v\|_2 = -v^t S v \qquad \text{production} \tag{11}$$
$$- 2\nu_\mathrm{T}\|Z\|_\mathrm{F}^2 - \frac{4C_\mathrm{S}^4\Delta^4}{\nu_\mathrm{T}}\mathrm{Tr}^2(SZ) \qquad \text{dissipation}$$
$$+ \nabla\cdot Q \qquad \text{conservative term}$$
$$Q = 2\nu_\mathrm{T} v^t Z + 4\frac{(C_\mathrm{S}\Delta)^4}{\nu_\mathrm{T}}\mathrm{Tr}(S^t Z)\, v^t S - \frac{qv}{\rho} - \frac{1}{3}v\frac{\delta\Pi}{\delta u}v. \tag{12}$$

This equation is obtained by taking the dot product with v of Eq. (8) and integrating by parts. The right-hand side has three contributions: the first (production) is indefinite, the second (dissipation) is non-positive and the third (conservative) has the form of a divergence. The conservative term can contribute locally but has zero spatial average. We normalize the i-th Lyapunov field $\|v_i\|_2$ by its spatial average to obtain

$$\frac{D_t\|v_i\|_2}{2\langle v_i^t v_i\rangle_\mathrm{s}} = -\frac{v_i^t S v_i}{\langle v_i^t v_i\rangle_\mathrm{s}} - 2\nu_\mathrm{T}\frac{\|Z\|_\mathrm{F}^2}{\langle v_i^t v_i\rangle_\mathrm{s}} - \frac{4C_\mathrm{S}^4\Delta^4}{\nu_\mathrm{T}}\frac{\mathrm{Tr}^2(SZ)}{\langle v_i^t v_i\rangle_\mathrm{s}} + \frac{\nabla\cdot Q}{\langle v_i^t v_i\rangle_\mathrm{s}}. \tag{13}$$

With this definition of the Lyapunov field, $l(x,t) = D_t\|v_i\|_2/\langle v_i^t v_i\rangle_\mathrm{s}$, one has the intuitive relations

$$\langle l_i(x,t)\rangle_\mathrm{s} = \lambda_i(t), \qquad \langle l_i(x,t)\rangle_\mathrm{st} = \Lambda_i. \tag{14}$$

In practice, the Lyapunov fields are computed as the Floquet vectors of the UPO. The Floquet vectors are computed by Arnoldi iteration. For each iteration, we must compute the product of the Jacobian on a given perturbation vector, which is done by time-stepping Eqs. (4) and (8) along the UPO with the given perturbation as the initial condition $v(0)$. It took 2000 iterations to converge the first 500 Lyapunov exponents. The Lyapunov fields are reconstructed from the Floquet vectors by numerically approximating the material derivative in the definition. In addition, we computed the production term in Eq. (12) separately.

Due to the fact that the numerical data for the UPO are not perfectly periodic, the Lyapunov fields beyond the twentieth are inaccurate. They show a rapid transient at the beginning of the base orbit. The only remedy is to compute the UPO with greater accuracy. In the following, we will restrict the analysis of Lyapunov fields to the leading twenty

4. Results

The first 500 Lyapunov exponents are shown in Fig. 3, along with their cumulative sum. About 210 exponents are positive, and the integer part of the attractor dimension, determined by the zero crossing of the cumulative sum, is about 440. This number is in line with the observation of Léorat and Grappin [12] and Keefe *et al.* [13]. It also agrees with the idea that the attractor dimension correlates with DOF that are not strongly damped by the eddy viscosity. These would be the DOF inside a spherical shell in wave vector space of radius 6. As can be seen in Fig. 2, this is where the spectrum starts to deviate from Kolmogorov's -5/3 law.

The leading 24 time-local exponents are shown in Fig. 4. This includes all time-local exponents that are largest at some point along the UPO. The limitations of studying only the leading exponent and vector are obvious. This observation is in line with earlier work by van Veen *et al.* [19] on box turbulence at a lower Reynolds number. The data also indicate that the time-periodic flow has a relatively quiescent phase and a more active phase, the latter spanning $t/T = 5\ldots8$. The differences between the two phases are described in reference [18].

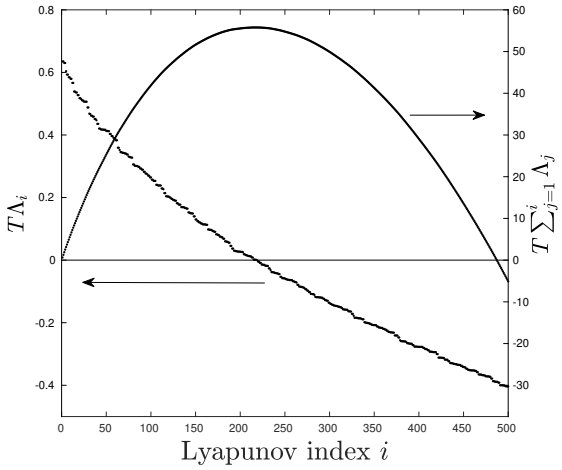

Figure 3. The first 500 Lyapunov exponents as computed from the Floquet spectrum. Also shown is the cumulative sum of Lyapunov exponents (scale on the right).

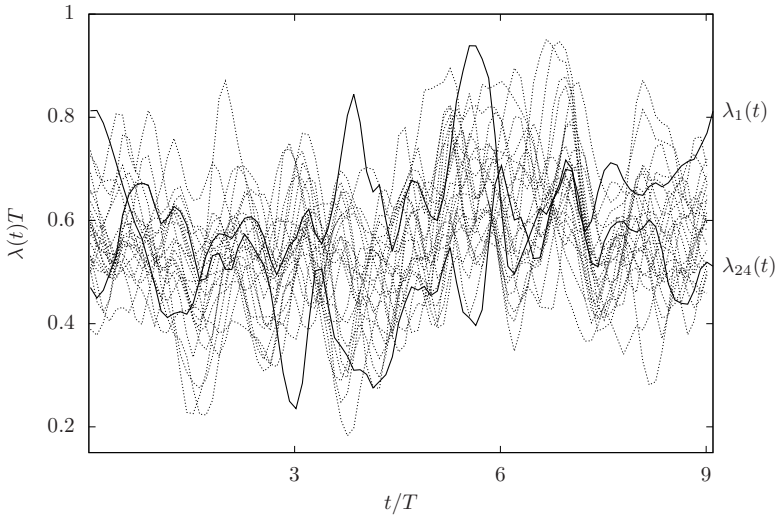

Figure 4. The leading 24 time-local Lyapunov exponents, normalised by the large eddy turnover time. The time-local exponent giving rise to the largest time-mean exponent, as well as the 24^{th} in the spectrum are shown with bold lines.

Next, we turn to the dynamics of vortices. In Fig. 5 four snapshots are shown, spanning nearly one large eddy turnover time. The blue surfaces are isosurfaces of enstrophy and mostly take the form of vortex pairs. In particular, we focus on the pair at the front face of the periodic cube, indicated by an arrow. The four frames show the pair developing an instability and then disintegrating. In order to make the link with the Lyapunov fields, we collapsed the top twenty fields into a "local maximum Lyapunov field" by selecting the maximal $l(x,t)$ at each point on the spatial grid and at each time instant. The result is a continuous, but not smooth, field of which isosurfaces are shown. The isosurfaces have been coloured corresponding to the Lyapunov index of the maximizing field. If the isosurface is white, the leading instability corresponds to the first Lyapunov field and if it is red to the twentieth.

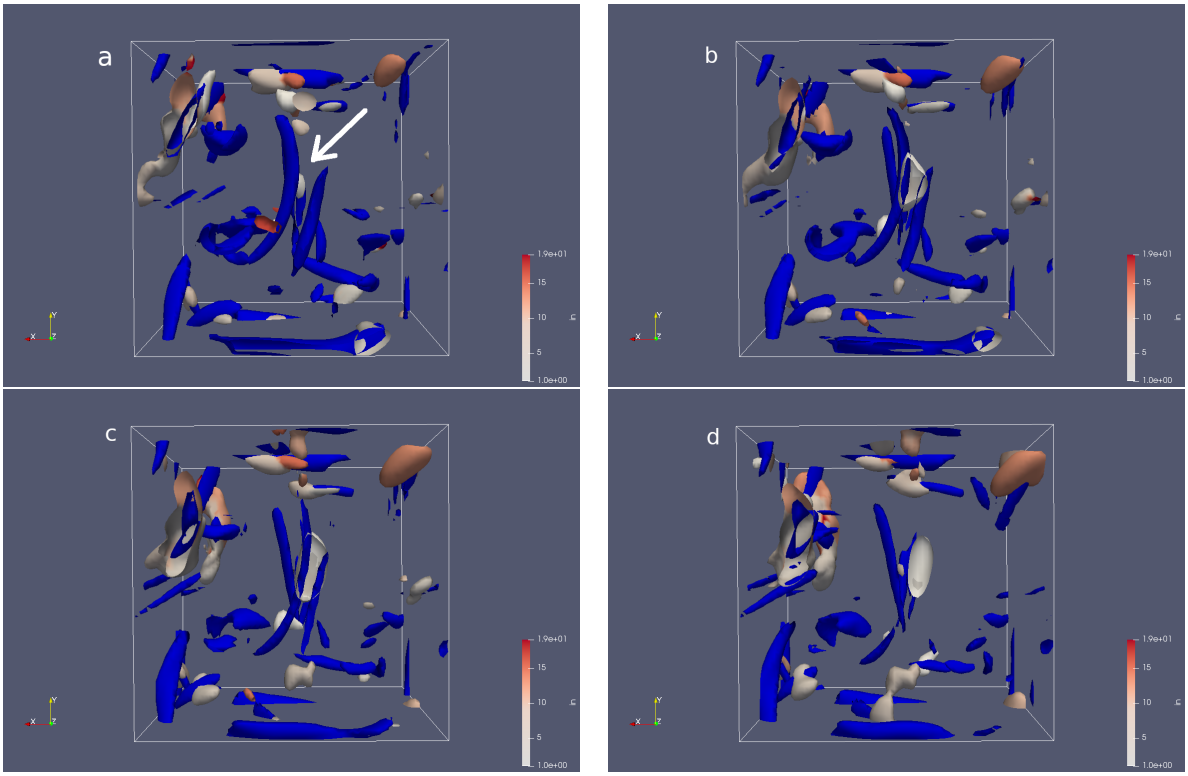

Figure 5. Four snap shots of along the UPO about $0.25\,T$ apart. Shown are the isosurfaces of enstrophy at 50% of its maximum value in blue and the local maximal Lyapunov field at 25% of its maximal value. The latter are shown in a scale of white (Lyapunov index 1) to red (Lyapunov index 20). See text for the definition of the local maximal Lyapunov field. Frames (a)–(d) show the instability and decay of a pair of counter rotating vortices. Note, that the front face of the periodic cube slices through the isosurface of the local maximal Lyapunov field.

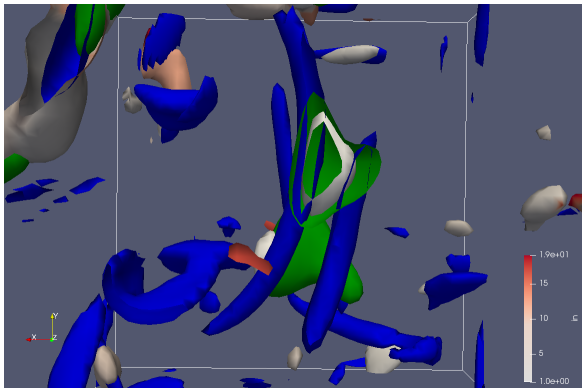

Figure 6. Zoom of frame (b) of Fig. 5 with added in green isosurfaces of the production term in Eq. (12) at 25% of its peak value. The largest perturbation growth occurs in the high strain region in between the vortices.

From frame 5(a) to frame 5(b) the vortex pair develops an instability tied to the leading Lyapunov field. It is localized in the high-strain region between the counter rotating vortices. From frame 5(b) to frame 5(c) the vortices have weakened and in frame 5(d) they have disintegrated. We would expect to see smaller vortical structures replace them, completing one step of the hypothetical energy cascade across length scales. Probably owing to the narrow inertial range in this flow, no clear smaller-scale structures are observed. Instead, the eddy viscosity appears to dissipate the energy carried by the vortex pair.

If the contribution from the conservative term in Eq. (12) can be neglected, the only source of perturbation growth is the production term. In order to verify this, we computed it separately and plotted it isosurface along with that of the local maximum Lyapunov field. The result, shown in Fig. 6, confirms that there is a strong correlation between the two. Here, the Lyapunov field is approximately aligned with the leading eigenvector of the rate-of-strain tensor.

5. Discussion

Using the Floquet spectrum of a UPO embedded in LES turbulence, we have started to investigate the time- and space-local Lyapunov fields and their connection to the dynamics of coherent structures. The complexity of the turbulent flow is evident from the number of unstable Lyapunov exponents, over 200, and the geometric attractor dimension (over 450), in line with previous studies [12, 13]. As was expected from earlier studies [19, 15], we show that a large number of Lyapunov fields can give the fastest perturbation growth at a given point in space and a given instant in time – in this flow at least 24. We collapsed the time and space resolved data of the leading 20 Lyapunov fields into one field that gives the optimal perturbation. This quantity shows a strong correlation with the vortical structures. In particular, an instability appears in between two counter-rotating vortices about half a large eddy turnover time before their demise. Unfortunately, the inertial range in the LES turbulence is too narrow to see the emergence of smaller scale structures taking energy from the larger vortex pair.

In ongoing work we are re-computing the time-periodic base orbit with greater accuracy. This will allow us to compute a larger part of the Lyapunov spectrum accurately and, hopefully, verify the hyperbolic nature of coherent structures in the inertial range that is suggested by shell-model turbulence [14]. Another important improvement would be to recompute the UPO at a higher Reynolds number, allowing for the study of the generation of small vortical structures from larger ones. As explained in reference [18] progress is slow because of essential difficulties with the numerical methods when applied to high Reynolds number flows.

Acknowledgements

This research was partially funded by the COTURB program of the European Research Council (ERC-2014.AdG-669505). LvV was supported by an NSERC Discovery Grant (nr. 355849-2019). GK was supported by the Grant-in-Aid for Scientific Research program of the Japan Society for the Promotion of Science (nos. 25249014, 26630055). We are grateful to Daniel Chung for his careful revision of the manuscript.

References

[1] J. Jiménez, Coherent structures in wall-bounded turbulence, *J. Fluid Mech.* **842** (2018), P1.
[2] D. Kang, D. Yun and B. Protas, Maximum Amplification of Enstrophy in 3D Navier-Stokes Flows, preprint, *ArXiv:* physics.flu-dyn/1909.00041.
[3] M. P. Brenner, S. Hormoz and A. Pumir, Potential singularity mechanism for the Euler equations, *Phys. Rev. Fluids* **1** (2016), 084503.
[4] M. A. Liapounoff, Problème Général de la Stabilité du Mouvement, *Annales de la faculté des sciences de Toulouse* 2^e *série*, **9** (1907), 203–474.

[5] V. I. Oseledets, A multiplicative Ergodic Theorem. Characteristic Lyapunov exponents of dynamical systems, *Tr. Mosk. Mat. Obs.*, **19** (1968), 179–210 (in Russian). See also: L. Barreira and Y. Pesin, *Introduction to Smooth Ergodic Theory*, Graduate Studies in Mathematics **148**, AMS (2013).
[6] M. Sano and Y. Sawada, Measurement of the Lyapunov Spectrum from a Chaotic Time Series, *Phys. Rev. Lett.* **55** (1985), 1082–1085.
[7] A. Wolf, J. B. Swift, H. L. Swinney and J. A. Vastano, Determining Lyapunov exponents from a time series, *Physica D* **16** (1985), 285–317.
[8] F. Ginelli, P. Poggi, A. Turchi, H. Chaté, R. Livi and A. Politi, Characterizing Dynamics with Covariant Lyapunov Vectors, *Phys. Rev. Lett.* **99** (2007), 130601.
[9] F. Ginelli, H. Chaté, R. Livi and A. Politi, Covariant Lyapunov vectors, *J. Phys. A: Mat. Theor.* **46** (2013), 254005.
[10] K. A. Takeuchi, F. Ginelli, and Hugues Chaté, Lyapunov Analysis Captures the Collective Dynamics of Large Chaotic Systems, *Phys. Rev. Lett.* **103** (2009), 154103.
[11] D. Ruelle, Large volume limit of the distribution of characteristic exponents in turbulence, *Commun. Math. Phys.* **87** (1982), 287–302.
[12] R. Grappin and J. Léorat, Lyapunov exponents and the dimension of periodic incompressible Navier-Stokes flows: numerical measurements, *J. Fluid Mech.* **222** (1991), 61–94.
[13] L. Keefe, P. Moin and K. Kim, The dimension of attractors underlying periodic turbulent Poiseuille flow, *J. FLuid Mech.* **242** (1992), 1–29.
[14] M. Yamada and Ohkitani, K., The inertial subrange and non-positive Lyapunov exponents in a fully-developed turbulence, *Prog. Theor. Phys.* **79** (1988), 265–268.
[15] M. Inubushi, S.-i. Takehiro and M. Yamada, Regeneration cycle and the covariant Lyapunov vectors in a minimal wall turbulence, *Phys. Rev. E* **92** (2015), 023022.
[16] J. Smagorinsky, General circulation experiments with the primitive equations. I. The basic experiment, *Mon. Weather Rev.* **91** (1963), 99–164.
[17] M. Linkmann, M. Buzzicotti and L. Biferale, Multi-scale properties of large eddy simulations: correlations between resolved-scale velocity-field increments and subgrid-scale quantities, *J. Turbul.* **19** (2018), 493–527.
[18] L. van Veen, A. Vela-Martín and G. Kawahara, Time-periodic inertial range dynamics, *Phys. Rev. Lett.* **123** (2019), 134502.
[19] L. van Veen, S. Kida and G. Kawahara, Periodic motion representing isotropic turbulence, *Fluid Dyn. Res.* **38** (2006), 19–46.